Journal of the Mechanics and Physics of Solids 70 (2014) 136–153

Contents lists available at ScienceDirect

Journal of the Mechanics and Physics of Solids

journal homepage: www.elsevier.com/locate/jmps

Coupled glide-climb diffusion-enhanced crystal plasticity

M.G.D. Geers [a,*], M. Cottura [a], B. Appolaire [b], E.P. Busso [c,d], S. Forest [d], A. Villani [d]

[a] Eindhoven University of Technology, Department of Mechanical Engineering, Den Dolech 2, 5612 AZ Eindhoven, The Netherlands
[b] Laboratoire d'Etude des Microstructures, CNRS/Onera, BP72, 92322 Châtillon Cedex, France
[c] ONERA, BP 80100, 91123 Palaiseau Cedex, France
[d] Mines ParisTech, Centre des Matériaux/CNRS, UMR 7633, BP87, 91003 Evry Cedex, France

ARTICLE INFO

Article history:
Received 24 January 2014
Received in revised form
11 April 2014
Accepted 12 May 2014
Available online 21 May 2014

Keywords:
Crystal plasticity
Dislocation climb
Vacancy diffusion
Dislocation pile-ups
Strain gradient

ABSTRACT

This paper presents a fully coupled glide-climb crystal plasticity model, whereby climb is controlled by the diffusion of vacancies. An extended strain gradient crystal plasticity model is therefore proposed, which incorporates the climbing of dislocations in the governing transport equations. A global–local approach is adopted to separate the scales and assess the influence of local diffusion on the global plasticity problem. The kinematics of the crystal plasticity model is enriched by incorporating the climb kinematics in the crystallographic split of the plastic strain rate tensor. The potential of the fully coupled theory is illustrated by means of two single slip examples that illustrate the interaction between glide and climb in either bypassing a precipitate or destroying a dislocation pile-up.

1. Introduction

Many metallic systems are nowadays operated in a regime where the evolving mechanical properties do not just depend on dislocation glide mechanisms within the underlying crystals. This is typically the case for climb-assisted and creep deformation mechanisms, which are well known to contribute significantly at higher temperatures in pure metals (Seidman and Balluffi, 1966a,b; Dobson et al., 1967), solid solution alloys (Mohamed and Langdon, 1974), particle strengthened and multi-phase metals (Arzt and Wilkinson, 1986; Beddoes et al., 1995; Koch, 1998). Moreover, in modern thin film systems for micro-electronics or micro-electro-mechanical systems (MEMS), climb mechanisms already contribute to a significant extent at only mildly elevated temperatures (Legoues et al., 1990; Guo et al., 2010; Karanjgaokar et al., 2012) or even room temperature, e.g. in metallic interfaces (Wang et al., 2009; Wang and Pan, 2011).

Basic physical concepts of dislocation climb go back to the founding contributions of Hirth and Lothe (Lothe, 1960; Lothe and Hirth, 1967; Hirth and Lothe, 1968; Nix et al., 1971) and the work of Thomson and Balluffi (1962) on a kinetic theory for dislocation climb. Early work on the interaction (or transition) between glide and climb for solid solution alloys (mostly at higher temperatures) can be found in Mohamed and Langdon (1974). Dislocation climb requires particular attention in the study of interfaces, even at room temperature, see e.g. the work of Wang et al. (2009), Wang and Pan (2011), Wang and Misra (2011). The incorporation of atomistic aspects has been addressed by Lau et al. (2009) and Kabir et al. (2010), for BCC Fe within the power-law creep regime. Particular emphasis was placed on vacancy diffusion in FCC metals by Ortega et al.

* Corresponding author.
E-mail address: m.g.d.geers@tue.nl (M.G.D. Geers).
URL: http://www.tue.nl/mechmat (M.G.D. Geers).

http://dx.doi.org/10.1016/j.jmps.2014.05.007
0022-5096/

(2002), using a Molecular Dynamics (MD) approach, which might be of interest to determine the diffusion coefficients. A theoretical model in which the climb of dislocations is controlled by vacancy emission from extended jogs has been proposed by Argon and Moffatt (1981). The classical modeling of dislocation climb based on a continuous description of vacancy diffusion has been compared to atomistic simulations of dislocation climb in body-centered cubic iron under vacancy supersaturation by Clouet (2011).

To investigate the effect of climb on the collective behavior of dislocations, a number of papers have been published on the coupling of dislocation climb to discrete dislocation dynamics (DDD), e.g. see the work of Raabe (1998), Mordehai et al. (2008) and Ayas et al. (2014). Simplifying assumptions are thereby often made to enable computations to become feasible (e.g. time scale separation by considering a steady-state vacancy flux at each time step; ignoring the elastic interaction energy between dislocations and vacancies; assuming diffusion coefficients to be independent of stress). A DDD-analysis of the effect of climb on dislocation mechanisms and creep rates in superalloys was performed by Haghighat et al. (2013). Furthermore, a dislocation climb model based on coupling the vacancy diffusion theory with 3D discrete dislocation dynamics has been proposed by Gao et al. (2013) and Ayas et al. (2014). Recent DDD-based models coupling glide with climb have been published by Gao et al. (2011a), Keralavarma et al. (2012) and Danas and Deshpande (2013). For thin film problems, coupled DDD models have been proposed and assessed by Ayas et al. (2012) and Davoudi et al. (2012). Recent work has tried to incorporate as much as possible the basic processes occurring at the dislocation cores (Mompiou and Caillard, 2008; Gao et al., 2011b; Danas and Deshpande, 2013; Ayas et al., 2014; Geslin et al., 2014). The role of climb in evolving dislocation patterns has been shown in Bakó et al. (2006), even though the climb problem was solved in a more phenomenological manner (without coupling it to vacancy diffusion). The influence of climb on the back stress (past cuboidal particles) has been discussed by Rosler (2003), where the back stress was found to be proportional to the applied stress. Xiang and Srolovitz (2006) examined the effects of dislocation climb on bypassing particles, following a DDD approach.

To tackle larger length scales which cannot be investigated by atomistic or DDD models, the role of dislocation climb in plasticity has been addressed in several publications in a purely phenomenological manner, where constitutive equations incorporate the contribution of climb, e.g. see references cited in Gao et al. (2011b). The incorporation of climb in crystal plasticity has been dealt with in a phenomenological manner and improved versions thereof by Lebensohn et al. (2012).

The main objective of the present work is to break through the phenomenological nature of these approaches at the crystal plasticity level by coupling deformation to dislocation motion assisted by glide and diffusional climb. For this purpose, a state-of-the-art crystal plasticity model needs to be used, which properly incorporates short-range dislocation–dislocation interactions. The backbone of the crystal plasticity framework is based on the strain gradient crystal plasticity model proposed by Evers et al. (2004), Bayley et al. (2006), and Ertürk et al. (2009), enriched with dislocation transport physics (Groma et al., 2003; Yefimov et al., 2004).

A second (physical) coupling is made here to link climb with vacancy diffusion. Reference to this is made to the work of Gao and Cocks (2009), which presents a thermodynamically based variational framework that links the climb of a single edge dislocation to the diffusion of vacancies. Attention is given to the governing equations and physics of the vacancy diffusion process, the driving forces acting on a dislocation to climb and the intrinsic coupling between both. The climb law is therefore diffusion-controlled.

The innovative contributions of the present paper are: (1) a physically based constitutive framework coupling vacancy diffusion to dislocation climb within a crystal plasticity setting; (2) the incorporation of climbing dislocations in the governing transport equations used in strain gradient crystal plasticity; (3) a global–local approach to separate the scales and assess the influence of the local diffusion problem on the global plasticity problem; and (4) an enrichment of the crystal kinematics, enabling the incorporation of the climb kinematics in the crystallographic split of the plastic strain rate tensor.

Section 2 introduces the governing equations for vacancy diffusion and the adopted strain gradient crystal plasticity model. Section 3 presents the coupling between climb and glide, which entails the modified diffusion problem and the modified crystal plasticity problem. Section 4 provides some illustrative single slip case studies highlighting the interaction between diffusion, climb, and glide. Finally, the conclusions are presented in Section 5.

2. Model formulation

2.1. Main physical concepts

The interaction between vacancy diffusion and dislocation climb has been studied at the level of individual and discrete dislocations by Gao and Cocks (2009). At this level, henceforth called ‘the local level’, a direct relation exists between the transport of vacancies and the dislocation climb process, involving absorption/emission of vacancies at jogs in the dislocation core. One of the key results is an expression of the local climb velocity as a function of the associated quantities, i.e. the local concentration gradient and the mean concentration along the dislocation core. This mean concentration depends on the configurational forces acting on the dislocation (see e.g. Gao and Cocks, 2009; Danas and Deshpande, 2013), composed of the following contributions: (1) the so-called osmotic force, which results from the change of free energy upon creating or removing vacancies during dislocation climb; (2) the drag force acting on the dislocation, which results from the change of free energy of vacancies due to the pressure evolution during dislocation climb (see Section 3.1); and (3) the climb component F_c of the Peach–Koehler force.

The Peach–Koehler force is given by

$$\vec{F}_{PK} = b\,(\boldsymbol{\sigma}\cdot\vec{m})\times\vec{p} \tag{1}$$

with b the Burgers vector length, $\vec{m}$ the glide direction, $\vec{n}$ the slip plane normal and $\vec{p}=\vec{m}\times\vec{n}$. The tensor $\boldsymbol{\sigma}$ is the total Cauchy stress tensor, i.e. the sum of the stress due to the external load and the internal stress due to e.g. short range dislocation interactions. The component contributing to climb (acting along the direction $\vec{n}$) then reads

$$F_c = \vec{F}_{PK}\cdot\vec{n} = b\,[(\boldsymbol{\sigma}\cdot\vec{m})\times\vec{p}\,]\cdot\vec{n} \tag{2}$$

We will study the problem at the meso-scale, where pile-ups against particles can be resolved explicitly so that it is meaningful to establish a direct coupling between the mean vacancy flux and the dislocation climb process. We limit ourselves to 2D problems governed by edge dislocations only. At that scale, the total amount of dislocations is split in a positive fraction ρ_+ and a negative fraction ρ_-. The sign of the dislocation results from the position of the extra half-plane with respect to the slip plane normal, or alternatively, with the orientation of the Burgers vector with respect to the slip orientation vector. The difference between ρ_+ and ρ_- gives the density of the geometrically necessary dislocations $\rho_G=\rho_+-\rho_-$ (GNDs) and the total dislocation density ρ, which is the sum $\rho=\rho_++\rho_-$. The dislocation problem can be described in a fully conservative manner with transport equations. Since the analysis is carried out at the meso-scale, all dislocations are assumed to participate in the climbing process. The corresponding dislocation transport equations have to be updated to incorporate the contribution through climbing.

2.2. Governing equations for vacancy diffusion

The thermodynamical setting for the vacancy diffusion problem is typical for a standard diffusion problem. This subsection focuses on the governing equations for the diffusion problem. The governing quantities and field variables, along with their notations, are

- vacancy concentration = vacancy volume fraction, c [–]
- volumetric vacancy flux, $\vec{J}_v$ [m/s]
- mobility, M [m^5/ Js]
- vacancy diffusion constant, D [m^2/s]
- molar volume, V_m [m^3/mol]
- relaxed volume per mole of vacancies, ΔV_r [m^3/mol]
- molar vacancy formation energy, Q_v [J/mol]
- diffusion potential, μ_v [J/m^3] or [N/m^2] or [Pa]
- absolute temperature, T [K]
- universal gas constant, R [J/(K mol)]

For a definition of the diffusion potential, here denoted μ_v, refer to the work of Larché and Cahn (1985). The local conservation of mass, or continuity equation, reads

$$\dot{c} = -\vec{\nabla}\cdot\vec{J}_v \tag{3}$$

A linear relation is classically postulated to hold between the vacancy flux and the driving force for diffusion:

$$\vec{J}_v = -M\,\vec{\nabla}\mu_v \quad \text{in } V \tag{4}$$

The volumetric diffusional mobility M is related to the vacancy diffusion constant D (Gao and Cocks, 2009) by

$$M = \frac{DV_m}{RT}\,c\,(1-c) \tag{5}$$

Within a thermodynamical setting, assuming that vacancies constitute an ideal solid solution, the diffusion potential can be determined (e.g. Larché and Cahn, 1985; Gao and Cocks, 2009) as

$$\mu_v = \frac{RT}{V_m}\left(\ln\frac{c}{1-c}+\frac{Q_v}{RT}-\frac{1}{3}\frac{\mathrm{tr}(\boldsymbol{\sigma})\Delta V_r}{RT}\right) \quad \text{in } V \tag{6}$$

with the following boundary conditions (on the external boundary ∂V) for the diffusion potential μ_v (Gao and Cocks, 2009)

$$\mu_v = \vec{n}\cdot\boldsymbol{\sigma}\cdot\vec{n} \quad \text{on } \partial V \tag{7}$$

The origin of the different terms in (6) is

- $RT/V_m\ln(c/(1-c))$: entropy of mixing of the vacancies in the lattice
- Q_v: vacancy formation energy, i.e. the enthalpy change associated with the breaking of actual bonds in the region of the vacancy under zero local pressure (constant for a given crystal)
- $-\frac{1}{3}\mathrm{tr}(\boldsymbol{\sigma})\Delta V_r$: elastic energy released when an atom is removed locally, which is the negative work done by the local pressure

Particular emphasis has to be given to the coupling of vacancy diffusion with dislocation climb, i.e. how that reversely affects the transport of vacancies.

2.3. Governing crystal plasticity equations

A rate-dependent crystal plasticity formulation is adopted, where dislocations are assumed to be mobile during deformation. The problem will be studied in the adopted 2D setting, in which only edge dislocations are considered. For the present work, a small strain formulation is adopted. The classical governing equations for the glide only case are summarized next:

- The additive decomposition of the infinitesimal strain tensor $\boldsymbol{\varepsilon}$ into its elastic part $\boldsymbol{\varepsilon}_\mathrm{e}$ and its plastic part $\boldsymbol{\varepsilon}_\mathrm{p}$
$$\boldsymbol{\varepsilon} = \boldsymbol{\varepsilon}_\mathrm{e} + \boldsymbol{\varepsilon}_\mathrm{p} \tag{8}$$

- The constitutive equation, coupling the Cauchy stress tensor $\boldsymbol{\sigma}$ to the elastic strain tensor $\boldsymbol{\varepsilon}_\mathrm{e}$ through the FCC-anisotropic elastic fourth-order constitutive tensor ${}^4\boldsymbol{C}$
$$\boldsymbol{\sigma} = {}^4\boldsymbol{C} : \boldsymbol{\varepsilon}_\mathrm{e} \tag{9}$$

- The crystallographic split, coupling the plastic strain rate tensor $\dot{\boldsymbol{\varepsilon}}_\mathrm{p}$ to the crystallographic slip rates $\dot{\gamma}^\alpha$ and the symmetrized Schmid tensor $\mathbf{P}^\alpha = \frac{1}{2}\left(\vec{m}^\alpha \otimes \vec{n}^\alpha + \vec{n}^\alpha \otimes \vec{m}^\alpha\right)$, with $\vec{m}^\alpha$ and $\vec{n}^\alpha$ the slip direction and slip plane normal, respectively
$$\dot{\boldsymbol{\varepsilon}}_\mathrm{p} = \sum_\alpha \dot{\gamma}^\alpha \mathbf{P}^\alpha \tag{10}$$

When focusing on a single slip system only, the superscript α will be omitted. Rewriting the scalar climb component of the Peach–Koehler force (2) as a projection on the slip system gives

$$F_c = b\,[(\boldsymbol{\sigma} \cdot \vec{m}) \times \vec{p}\,] \cdot \vec{n} \tag{11}$$

$$F_c = b\,(\boldsymbol{\sigma} \cdot \vec{m}) \cdot (\vec{p} \times \vec{n}) = b\,(\boldsymbol{\sigma} \cdot \vec{m}) \cdot (-\vec{m}) \tag{12}$$

$$F_c = -b\,\boldsymbol{\sigma} : \vec{m} \otimes \vec{m} \tag{13}$$

We will next focus on the slip law defining $\dot{\gamma}$ and the dislocation transport equations. A viscous drag relation is applied between the average dislocation velocity field v and the driving force F_g acting on the dislocations (i.e. the glide component of the Peach–Koehler force):

$$v(x,t) = \frac{F_g}{B} \tag{14}$$

where the parameter B is the drag coefficient. The driving force acting on a dislocation consists of an elastic component emanating from the long range elastic fields and an internal stress component resulting from short-range dislocation interactions. Thus,

$$F_g(x,t) = b\,[\sigma_\mathrm{e} + \sigma_\mathrm{i}]. \tag{15}$$

In the above equation, the stress σ_e is the projection of the external stress vector (acting on the glide plane) on the glide direction, i.e. the externally resolved shear stress

$$\sigma_\mathrm{e} = [(\boldsymbol{\sigma}_\mathrm{e} \cdot \vec{m}) \times \vec{p}\,] \cdot \vec{m} \tag{16}$$

$$\sigma_\mathrm{e} = \vec{n} \cdot \boldsymbol{\sigma}_\mathrm{e} \cdot \vec{m} \tag{17}$$

The external stress tensor $\boldsymbol{\sigma}_\mathrm{e}$ corresponds to the stress defined in Eq. (9), whereby only the long range elastic fields are considered in $\boldsymbol{\varepsilon}_\mathrm{e}$. The internal stress σ_i results from the short range discrete interactions between dislocations, i.e. through a gradient in the GND density. The internal stress here reads

$$\sigma_\mathrm{i} = -\frac{G}{2\pi[1-\nu]}\frac{b}{\rho}\frac{\partial \rho_\mathrm{G}}{\partial x} = -\frac{G}{2\pi[1-\nu]}\frac{b}{\rho}\left(\frac{\partial \rho_+}{\partial x} - \frac{\partial \rho_-}{\partial x}\right) \tag{18}$$

whereby G is the shear modulus and ν Poisson's ratio. Note that this shear internal stress σ_i does not contribute to the climb component of the Peach–Koehler force F_c, since it cancels out in the projection used in Eq. (13). Eq. (18) was developed by Groma et al. (2003) and Yefimov et al., (2004), using statistical mechanics arguments applied to nearest neighbor interactions. Note also that similar dislocation interaction models exist, see Evers et al. (2004), Bayley et al. (2006), and Ertürk et al. (2009).

For simplicity, the classical Orowan relation for the slip rate $\dot{\gamma}$ is here adopted,

$$\dot{\gamma} = \rho b v \tag{19}$$

The balance equations for the glide-only problem are given by
(i) GND balance equation

$$\frac{\partial \rho_G}{\partial t} + \frac{\partial}{\partial x}(\rho v) = 0 \qquad \Leftrightarrow \qquad \frac{\partial \rho_+}{\partial t} - \frac{\partial \rho_-}{\partial t} + \frac{\partial}{\partial x}([\rho_+ + \rho_-]v) = 0 \tag{20}$$

This equation implies the conservation of the total Burgers vector (as can be verified by an integration over the entire domain).
(ii) balance of the total density of dislocations:

$$\frac{\partial \rho}{\partial t} + \frac{\partial}{\partial x}(\rho_G v) = s \quad \Leftrightarrow \quad \frac{\partial \rho}{\partial t} + \frac{\partial}{\partial x}([\rho_+ - \rho_-]v) = s \tag{21}$$

This second balance equation is a transport equation. It was proposed by Groma et al. (2003), using statistical mechanics arguments (for an extensive discussion on this second balance equation, see also Hirschberger et al., 2011). In the absence of a source or sink, i.e. $s=0$, Eq. (21) implies the local conservation of the total number of dislocations. Details on the role of the convective contribution in this term are discussed in Hirschberger et al. (2011). The coupled problem consisting of the two partial differential equations (20) and (21) describes the evolutionary behavior of all dislocations. The source and sink of dislocations are described by the source term s on the right-hand side of Eq. (21).

3. Coupled glide-climb crystal plasticity

3.1. Modified diffusion problem

In general, one has to distinguish two distinct limit regimes for the coupling between bulk vacancy diffusion and dislocation climb. To clarify this, the process at the core and dislocation line needs to be detailed. Among the three configurational forces expanding power during a dislocation climb process, mentioned in Section 2.1, the drag force induced by the elastic interaction between the dislocation and the vacancies can usually be neglected. Indeed, the contribution of $\mathrm{tr}(\boldsymbol{\sigma})\Delta V_r$ is much smaller than the work performed by the climb component of the Peach–Koehler force F_{PK} (see Gao and Cocks, 2009). Therefore, the last term in the diffusion potential μ_v in Eq. (6) can be dropped. The osmotic force per unit length of an edge dislocation F_o is directly related to the diffusion potential μ_v and equals $b\mu_v$. Using Eq. (6) in the dilute limit, i.e. $c_v \ll 1$, the osmotic force F_o is given by the expression proposed by Hirth and Lothe (1968)

$$F_o = \frac{R\,T\,b}{V_m} \ln\left(\frac{c^\star}{c_0}\right) \tag{22}$$

Here, $c^\star$ represents the vacancy concentration in the core of the dislocation, whereas $c_0 = \exp(-Q_v/RT)$ is the standard-state concentration of vacancies (i.e. the equilibrium concentration at temperature T if no dislocations are present). Neglecting the drag force, the total force that expands power when a dislocation climbs is then given by

$$F = F_c + F_o = F_c + \frac{R\,T\,b}{V_m} \ln\left(\frac{c^\star}{c_0}\right) \geq 0 \tag{23}$$

When $F=0$, the dislocation core is at local equilibrium and

$$c^\star = c_{eq} = c_o \exp\left(-\frac{F_c V_m}{bRT}\right) \tag{24}$$

In that case, vacancy dynamics (creation and destruction) is fast at jogs and the equilibrium concentration c_{eq} is therefore easily maintained at a jog. The concentration at the core $c^\star$ depends on the jog content and spreading. If the mean free path of the vacancies along the dislocation line is larger than the jog spacing, then the whole dislocation line will have a vacancy concentration nearly equal to c_{eq} (and $F=0$). In such case, the rate of vacancy absorption is then only limited by the vacancy bulk diffusion rate towards the dislocation. This is the *diffusion-limited* regime. For this regime, the dislocations locally maintain the equilibrium concentration c_{eq} in the core, which is directly related to the climb component of the Peach–Koehler force acting on it.

If the mean free path is smaller than the jog spacing (either because diffusion along the core is slow or there are few jogs), then the rate of vacancy absorption is limited by the rate at which vacancies are absorbed at the jogs along the dislocation line. This is the *sink-limited* regime. In this regime, an expression relating the driving force F and the climb velocity must be provided on the basis of the elementary processes acting at the dislocation core. By eliminating c_0 in Eq. (23) by making use of Eq. (24), the following expression for the driving force results $F = RTb/V_m \ln(c^\star/c_{eq})$. As usually done in irreversible thermodynamics, if F is not too large a linear relationship between the climb velocity v_c and F can be postulated, i.e. $v_c = K_c F$ where K_c is a positive kinetic coefficient. This amounts to add to the dissipation potential Ψ in Gao and Cocks (2009) a term quadratic in the climb velocity. It is worth noting that if $c^\star$ is close to c_{eq}, F can be linearized with respect to the concentrations as $F = RTb/V_m\,(c^\star - c_{eq})$. Then, the climb velocity and the flow of vacancies are proportional to

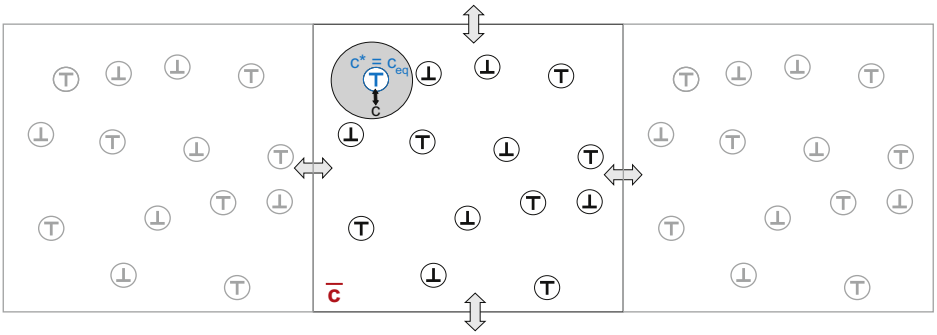

Fig. 1. Global and local scales for diffusional climb.

$c^\star - c_{eq}$ as in Ayas et al. (2012) and Danas and Deshpande (2013). The extension of the present model to the sink-limited regime in this manner is thus straightforward, since it changes only the climb velocity at the discrete dislocation level, Eq. (33). The required additional equation for $c^\star$ can be easily obtained following the procedure proposed by Danas and Deshpande (2013) and Ayas et al. (2012), see e.g. Eq. (13) in Danas and Deshpande (2013) (in which c_0 is here $\bar{c}$ and in which $\bar{c}$ is here $c^\star$).

Depending on the material properties controlling the processes at the dislocation cores (diffusion, jog nucleation, vacancy emission/absorption), one of the two regimes mentioned can be considered as operating during a whole process. These properties are not always trivial quantities to identify. Any mechanism that promotes the diffusion along the core or the dislocation line will favor the diffusion-limited regime. Since pipe diffusion is known to be significant in many cases, we consider the diffusion-limited regime as the most relevant one here.

A local and a global scale need to be distinguished next. The local scale is that of the discrete dislocation, for which we will denote the vacancy concentration field in its neighborhood simply by c. The global scale corresponds to that of a macroscopic material point with its connected unit cell or representative volume element (RVE). The RVE is the representative material volume within which local dislocations reside, represented by a dislocation density ρ, see Fig. 1.

The average vacancy concentration in that RVE is denoted $\bar{c}$. The transport of vacancies across the RVE boundaries has to be solved by a global diffusion equation applied to the global $\bar{c}$, reflecting the variations in the mean vacancy concentration between neighboring RVEs. Note that mean-field assumptions only apply to the global scale, since the solution of the local scale problem will be done analytically. In summary, it is assumed that

- Macroscopic quantities associated with the material point are considered constant with respect to the RVE.
- Dislocations with a given sign within the RVE are equivalent. They are exposed to the same macroscopic fields and the local vacancy concentrations surrounding them are identical.
- All local problems related to individual dislocations in the RVE are identical, as a result of the mean field assumption adopted. Hence, all positive dislocations will have the same climb velocity. Likewise for the negative dislocations, where the climb velocity will be equal and opposite to the positive ones.

3.1.1. *The local problem*

The local problem aims to determine the amount of vacancies consumed or emitted by all the dislocations, which should be used as a source term in the global problem.

At the level of a single positive dislocation, whereby the core is enclosed within Γ (a cylindrical surface of unit length, with a unit normal vector $\vec{N}$ pointing inwards towards the core), the coupling with the local climb velocity v_c [m/s] can be expressed as

$$v_c = \frac{1}{b}\oint_\Gamma \vec{J}_v \cdot \vec{N}\, d\Gamma \tag{25}$$

which needs to be solved to extract the effective climb velocity resulting from the diffusion of vacancies into the dislocation core. Note that the dislocation line length considered in Eq. (25) is a unit length. Eq. (25) also shows that the core of a positive dislocation that climbs upwards (positive v_c) is a vacancy sink. Likewise, a negative dislocation is a vacancy source if it climbs upwards.

Consider a small cylindrical volume B at the local scale, and a single slip system with crystallographic unit directional vectors $\vec{n}, \vec{m}, \vec{p}$. The dislocation density ρ_+ is the total line length of positive edge dislocations per unit volume. The total dislocation line length in the volume B is L. The climbing dislocations in volume B are considered as point sources or sinks.

Using a continuum setting and considering all climbing dislocations as points sources or sinks allows us to apply Eq. (25) to the considered volume B. Eq. (25) reveals the inward flux into the core, i.e. a positive flux implies a decrease of the vacancy concentration in the vicinity of the core. Considering the climb velocity as a field property (i.e. constant in B) then

leads to

$$\int_B \dot{c}\, dB = -L\, v_c\, b \tag{26}$$

Recognizing that the sum of all the dislocation line lengths (of all dislocations in B) is the integrals of $\rho_+ dB$ over the volume B, allows us to rewrite Eq. (26) as

$$\int_B \dot{c}\, dB = -\int_B \rho_+ v_c\, b\, dB \tag{27}$$

Here, the climb velocity, v_c, acts along the normal direction $\vec{n}$. Evidently, the dislocation density ρ_+ in Eq. (27) corresponds to that of the climbing ones. Within the adopted mean field approach, all dislocations in the volume contribute to climb. Since Eq. (27) has to hold for any choice of B, the following continuum coupling equation for the local concentration of vacancies results

$$\dot{c} = -\rho_+ v_c\, b \tag{28}$$

We now incorporate both positive and negative dislocations (each with positive densities ρ_+ and ρ_-, respectively), since their climbing velocities have opposite sign under the influence of the same climb force. Hence, Eq. (28) reads

$$\dot{c} = -(\rho_+ v_c^+ - \rho_- v_c^-)\, b \tag{29}$$

with v_c^+ and v_c^- the climb velocities of the positive and negative dislocations, respectively. Eq. (29) clearly shows that a positive dislocation climbing up under the influence of a compressive σ_{mm} stress (with a positive climb velocity) consumes vacancies, through which the local vacancy concentration will decrease, thus resulting in a negative $\dot{c}$. Likewise, a negative dislocation in the same volume subjected to a compressive σ_{mm} stress will climb down with a negative velocity, contributing equally to a decrease in the local vacancy concentration.

The local evolution of c enters the global scale through a source term S_v given by the right-hand side of Eq. (29), depending on the net dislocation flux $\rho_+ v_c^+ - \rho_- v_c^-$, that has entered (or left) the global volume element through climb. This source term reads

$$S_v = -(\rho_+ v_c^+ - \rho_- v_c^-)\, b \tag{30}$$

As emphasized later in the text, under the influence of the same stress (and hence climb force), negative dislocations will always experience a climb velocity that is equal and opposite to that of positive dislocations. This consideration holds within the considered volume element representing a single material point. Hence, Eq. (30) can also be formulated as

$$S_v = -\rho\, v_c^+\, b \tag{31}$$

3.1.2. The global problem

The flux of climbing dislocations (positive or negative) $\rho_+ v_c^+ - \rho_- v_c^-$ appearing in the source term S_v at the global level depends on the rate of change $\dot{\bar{c}}$ and the local equilibrium concentration at the level of the discrete dislocations:

$$\rho v_c^+ = \rho_+ v_c^+ - \rho_- v_c^- = f(\dot{\bar{c}}, c_{eq}) \tag{32}$$

If the global vacancy concentration $\bar{c}$ equals the local equilibrium concentration c_{eq} (given by Eq. (24)), then climb should stop. Based on the solution of a stationary problem in a hollow cylinder, Bakó et al. (2011) proposed an expression for the climb velocity of dislocations, precisely satisfying this requirement. The climb velocity is determined at the level of the discrete dislocations, yielding

$$v_c = \frac{2\,\pi\, D\, c_0}{b\, \ln(r_\infty / r_c)} \left[\frac{c_{eq}}{c_0} - \frac{\bar{c}}{c_0} \right] \tag{33}$$

Here, the radius r_∞ is the distance at which it can be assumed that the local concentration c equals $\bar{c}$. A typical value for r_∞ is half the dislocation spacing, i.e. $r_\infty = 1/(2\sqrt{\rho})$. The core radius r_c is typically taken as $r_c = 4b$. The sign of the climb velocity in the climb direction depends on the dislocation sign and on the sign of the climb force acting on the dislocation. Note that the climb velocity is coupled to the stress state through c_{eq} via Eq. (24). It should be recalled that the climb contribution of the Peach–Koehler force under normal loading in the glide direction $\vec{m}$ equals $F_c = -b\, \sigma_{mm}$. To illustrate the possible climb configurations that a pair of dislocations, either positive or negative, may adopt, the climb directions and evolution of corresponding vacancy concentrations are schematically shown in Fig. 2.

Under compression in the $\vec{m}$ direction, σ_{mm} is negative. Hence, positive dislocations with a climb direction that is positively oriented with respect to $\vec{m}$ will have a positive climb velocity (upward climb, in the direction of $\vec{n}$). Likewise, negative dislocations with a climb direction that is negatively oriented with respect to $\vec{m}$ will have a negative climb velocity (downward climb). If σ_{mm} reverses sign, then the climb velocities will switch sign as well, and so will the climbing fluxes $\rho_+ v_c^+$ and $\rho_- v_c^-$.

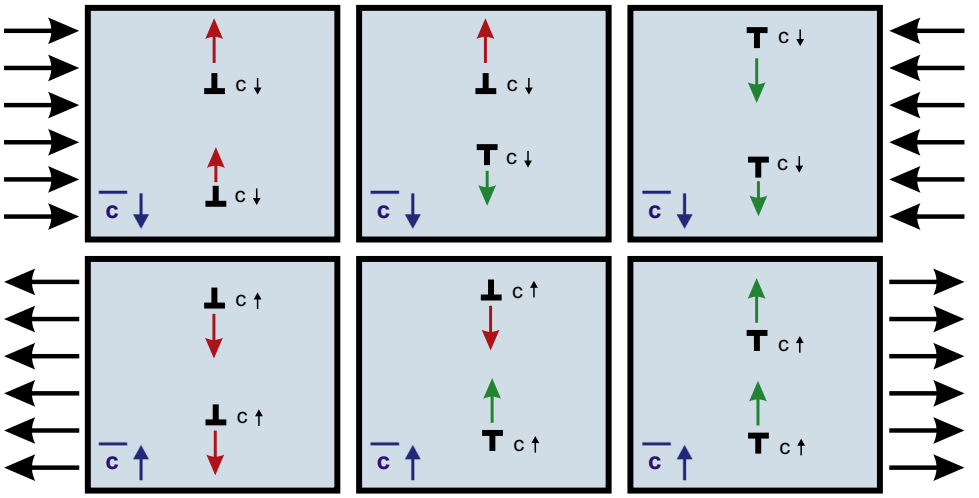

Fig. 2. Climb configurations under the influence of a normal stress σ_{mm}.

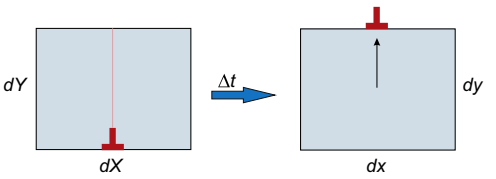

Fig. 3. Positive dislocation climbing over a distance dY in a volume $dV=dX\,dY$ during a time step Δt.

As climbing dislocations consume or emit vacancies, this process should enter the global diffusion problem through a source term, i.e.

$$\dot{c} = -\vec{\nabla}\cdot\vec{\boldsymbol{J}}_v + S_v \tag{34}$$

Here, S_v results from the local scale, including all the individual contributions of all dislocations in the volume element representing a global macroscopic point. This source term was expressed in Eq. (30) in terms of the positive and negative dislocations. With dislocation densities ρ_+, ρ_-, as well as the climb velocities known, Eq. (34) is now fully defined.

3.2. Modified crystal plasticity formulation accounting for dislocation climb

3.2.1. Climb contribution to the kinematic fields

In order to incorporate the effect of the dislocation climb on the plastic deformation tensor, the crystallographic split of the plastic strain rate tensor needs to be extended for the climb kinematics associated to each slip system.

The crystallographic split for $\dot{\boldsymbol{\varepsilon}}_{\mathrm{p}}$ used in Eq. (10) needs to be extended to account for the climb kinematics. Then,

$$\dot{\boldsymbol{\varepsilon}}_{\mathrm{p}} = \sum_\alpha \dot{\gamma}^\alpha \mathbf{P}^\alpha + \sum_\alpha \dot{\beta}^\alpha \mathbf{Q}^\alpha \tag{35}$$

in which the climb projection tensor $\mathbf{Q}^\alpha$ related to each slip system α reads

$$\mathbf{Q}^\alpha = \vec{m}^\alpha \otimes \vec{m}^\alpha \tag{36}$$

We next determine $\dot{\beta}^\alpha$ on the basis of the simple kinematics of a climbing dislocation on a single glide plane α, as represented in Fig. 3. The superscript α is henceforth omitted for brevity.

The height of the volume before and after climb is unaffected, i.e. $dy=dY$. The rate of change of the local vacancy concentration $\dot{c}$ is given by Eq. (28), which is evaluated over the time step Δt for the dislocation to climb over the vertical distance dY:

$$\dot{c} = -\rho_+ v_c^+ b \tag{37}$$

$$\Delta c = -\rho_+ (v_c^+ \Delta t)\, b \tag{38}$$

The volume occupied by the change in vacancies is denoted ΔV and directly results from the scalar change of the vacancy concentration Δc. Then,

$$\Delta V = \Delta c \, dX \, dY \tag{39}$$

The volume change ΔV can also be obtained from the deformed configuration $\Delta V = dx\, dy - dX\, dY$. When combined with Eq. (39)

$$dx\, dy - dX\, dY = \Delta c \, dX \, dY \tag{40}$$

$$(dx - dX)\, dY = \Delta c \, dX \, dY \tag{41}$$

$$\frac{dx - dX}{dX} = \Delta c \tag{42}$$

$$\beta = \varepsilon_{xx} = \Delta c \tag{43}$$

One finds, as expected, that the only kinematical contribution of the climbing dislocation is a normal strain ε_{xx} that exactly equals the local variation of the vacancy concentration. In a rate form, Eq. (43) gives the expected result for $\dot{\beta}$,

$$\dot{\beta} = \dot{c} = -(\rho_+ v_c^+ - \rho_- v_c^-)\, b \tag{44}$$

which can be directly used in the crystallographic split equation (35), whereby the solution of the local problem gives the flux of climbing dislocations.

3.2.2. Extended dislocation transport

The transport of dislocations through climb naturally modifies the balance equations (20) and (21). Taking into account the flux of positive and negative climbing dislocations, requires the balance equation for the total amount of dislocations to be extended. To clarify this point, we consider adjacent volume elements in Fig. 4 with a boundary through which the climbing flux may impact the vertical (climbing direction) redistributions of dislocations. Without any gradient in the densities of the positive (Fig. 4a) or negative (Fig. 4b) dislocations, an equal amount of dislocations leaving the top (or bottom) boundary will enter on the opposite bottom (or top) boundary. If so, the climb processes will affect the redistribution of vacancies but it will not on average change the dislocation densities. This is clearly different if a gradient exists along the climb direction for either the positive or the negative dislocations, as schematically depicted in the figure. The balance equation of the total amount of dislocations in a volume element, Eq. (21), is directly affected through these additional transport terms. The divergence of the flux of climbing dislocations should be added to Eq. (21), which for the single slip problem is limited to the gradient with respect to the vertical (climb) direction y. The resulting equation reads

$$\frac{\partial \rho}{\partial t} + \frac{\partial}{\partial x}([\rho_+ - \rho_-]v) + \frac{\partial}{\partial y}(\rho_+ v_c^+ + \rho_- v_c^-) = s \tag{45}$$

This balance equation follows directly from the inflow and outflow of dislocations in the considered central volume element. Recall that within the same volume element, subjected to the same stress (and hence climb force), the negative dislocations will always have a climb velocity that is equal and opposite to the climb velocity of the positive dislocations. This allows Eq. (45) to be rewritten as follows:

$$\frac{\partial \rho}{\partial t} + \frac{\partial}{\partial x}([\rho_+ - \rho_-]v) + \frac{\partial}{\partial y}([\rho_+ - \rho_-]v_c^+) = s \tag{46}$$

or expressed in terms of the density of geometrically necessary dislocations ρ_G

$$\frac{\partial \rho}{\partial t} + \frac{\partial}{\partial x}(\rho_G v) + \frac{\partial}{\partial y}(\rho_G v_c^+) = s \tag{47}$$

4. Single slip case studies

To illustrate the coupled framework and the interaction between glide and climb, we will present two 2D examples with a single slip system. The single glide plane case optimally focuses on the interaction between glide and climb (Ayas et al., 2012), since dislocations cannot glide past obstacles in 2D without climbing. Evidently, these results do not address the more complex physical behavior of climb for multiple glide systems but it does provide the best illustration of the proposed theory. The glide-climb problem considered is fully conservative, i.e. no sources or sinks for dislocations are incorporated and transport is therefore assumed to be dominant.

Since the relaxation of the elastic waves is by orders of magnitude faster than the evolution of plastic strain resulting from dislocation motion, static mechanical equilibrium will be assumed. At any time, the elastic strain can be computed by solving mechanical equilibrium at constant plastic strain. This is done iteratively using a fix point algorithm. A spectral method based on Fast Fourier Transforms (FFT) (Moulinec and Suquet, 1998) is employed to solve the governing equations.

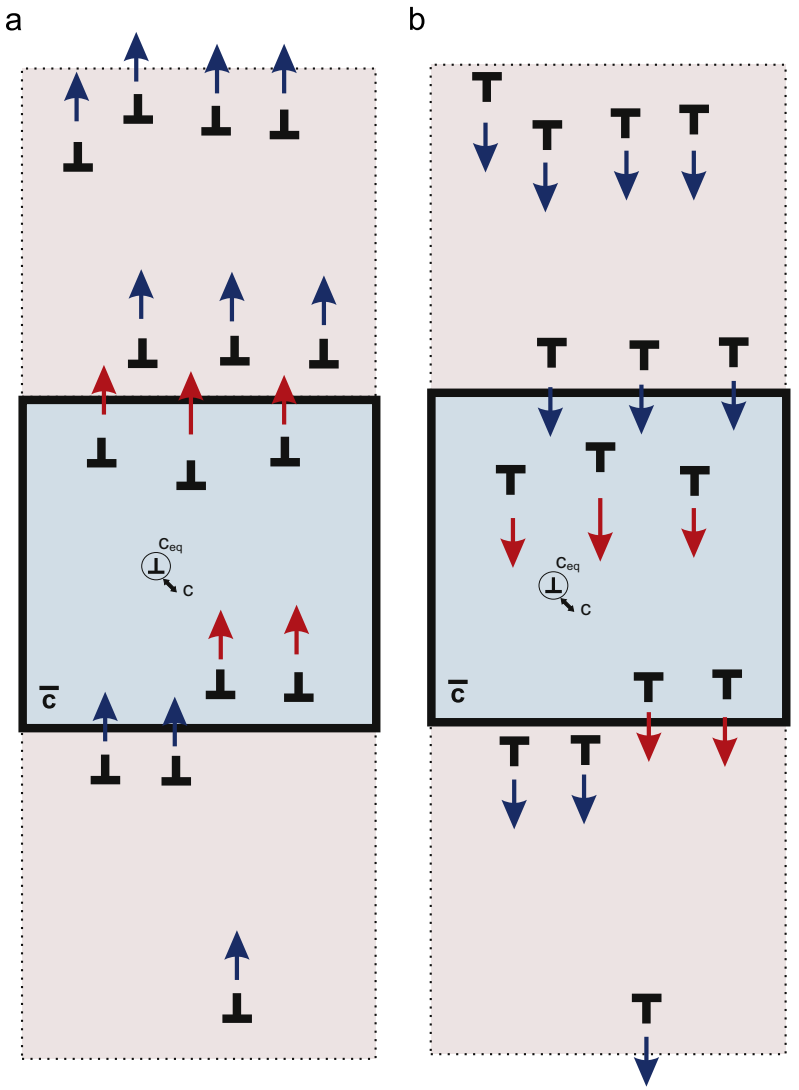

Fig. 4. Dislocation redistribution through climb in the presence of a vertical dislocation gradient. (a) Climb up, (b) climb down.

Table 1
Model parameters.

b (m)	B (Pa s)	D ($m^2\,s^{-1}$)	c_0	G (GPa)	ν
2.5×10^{-10}	10^{-3}	10^{-6}	10^{-4}	26.3	0.33

The dislocation densities and vacancy concentration evolution as well as the plasticity part of the problem are solved using an explicit time-stepping scheme. In addition, the convection-dominated problem represented by the dislocation density evolution equations (47) and (20) is solved with a first-order upwind scheme.

4.1. Model parameters

The material parameters adopted in the examples representative for the materials of interest (e.g. aluminum alloys) are presented in Table 1. Isotropic elastic moduli have been chosen for simplicity, since the effect of elastic inhomogeneities and anisotropy for these materials does not impact the presented results qualitatively. The value for the vacancy diffusivity has been chosen to illustrate the effect of dislocation climb relative to glide, inducing a climb rate that is three orders of magnitude smaller than the glide rate. This value is taken for numerical expediency only, whereby other values that are orders of magnitude lower give similar results in the considered configurations. Incorporating a realistic diffusivity, with a

dislocation climb rate that may be ten orders of magnitude smaller than the slip rate would require an adaptive scheme that allows for a distinct time step for climb and glide, as e.g. done in the work of Keralavarma et al. (2012).

All calculations have been performed with 256^2 nodes. It has been verified that the results are converged with respect to this spatial discretization because the differences are less than 0.1% compared with calculations carried out with 512^2 nodes.

4.2. Case study 1: elastic precipitate inside a plastic matrix

The first example aims to reveal the influence of climb on glide in the presence of a hard impenetrable precipitate. The addition of climb enables dislocations to escape from the pile-up by climbing over the precipitate. A periodic configuration of a circular elastic precipitate inside a plastic matrix is considered, see Fig. 5. The two-dimensional domain size is $4 \times 4\ \mu m^2$. The precipitate with diameter $D = 1.2\ \mu m$ is positioned at the center of the domain. A phenomenological phase field variable $\varphi(\vec{r})$ is used to describe the two-phase microstructure (with $\varphi = 0$ in the matrix, $\varphi = 1$ in the precipitate). In order to avoid numerical fluctuations, interfaces are smoothed over a width of 4 nodes. The precipitate is fully elastic with the same elastic moduli as its surrounding matrix (G and ν values are given in Table 1). The initial dislocations are homogeneously distributed in a horizontal band impinging the precipitate (Zone 1 in Fig. 5), whereas the rest of the matrix is initially dislocation-free (Zone 2 in Fig. 5). The width of Zone 1 equals $0.75\ \mu m$, thus assumed to be smaller than the particle diameter. If this width were either equal or larger than the particle diameter, then dislocations would be able to bypass the particle through glide only in a trivial manner, which would be of no interest to the present study. The initial dislocation density in the horizontal band equals $\rho_0 = 5 \times 10^{12}\ m^{-2}$, yielding an average total dislocation density of $\overline{\rho} = 7.5 \times 10^{11}\ m^{-2}$ for the entire domain. The total amount of dislocations is conserved, since sources and sinks are omitted in this analysis. Plasticity inside the matrix results from dislocation motion on one slip system oriented parallel to the x_1-direction. Periodic boundary conditions are used to solve the coupled problem. A global tensile shear deformation of $\overline{\varepsilon}_{12} = 10^{-3}$ is applied and maintained constant (relaxation test).

The prediction for the glide-only case will next be confronted with the climb-assisted glide case. The evolution of the geometrically necessary dislocation density field $\rho_G(\vec{r})$ and the plastic shear $\varepsilon^p_{12}(\vec{r})$ is presented in Figs. 6 and 7, respectively. At $t=0$ (not shown), there are no GND dislocations, since positive and negative dislocations are initially distributed homogeneously inside the horizontal band. Upon applying the load, positive dislocations move to the right while negative dislocations go to the left. Dislocations glide until they form pile-ups at the precipitate walls, as can be seen in the GND density distribution in Fig. 6 at $t = 0.5\ \mu s$. In the matrix Zone 2, there were no initial dislocations. At the onset of deformation, when glide is still the principal mechanism of dislocation motion, the dislocations in the two case studies exhibit similar behavior and reach comparable spatial distributions. After a certain time, the GND distribution does not evolve anymore since dislocation glide is restricted to the respective slip planes in the glide-only case. An equilibrium state is reached whereby dislocations are confined in Zone 1 against the precipitate (Fig. 6 – top). However, when dislocation climb is accounted for, the positive (respectively negative) dislocations piled-up on the upper half of the left (respectively right) wall of the precipitate and move up while the ones on the lower half move down (Fig. 6 – bottom). The GND density decreases, gradually destroying the pile-ups over time. Positive and negative dislocations are relocating in the same area above and below the precipitate.

The role of dislocation climb becomes even more apparent upon analyzing the evolution of the plastic shear strain field $\varepsilon^p_{12}(\vec{r})$, see Fig. 7. The previously described stages in dislocation motion explain the evolution observed. In the first stages after loading, the splitting of the positive and negative dislocations to the left and right sides of the precipitate walls generates a plastic shear strain in Zone 1 in both the glide-only and the climb-assisted glide case (Fig. 7). Since there are no initial dislocations in Zone 2, $\varepsilon^p_{12}(\vec{r})$ remains equal to zero. Once the pile-ups have formed, $\varepsilon^p_{12}(\vec{r})$ does not evolve anymore

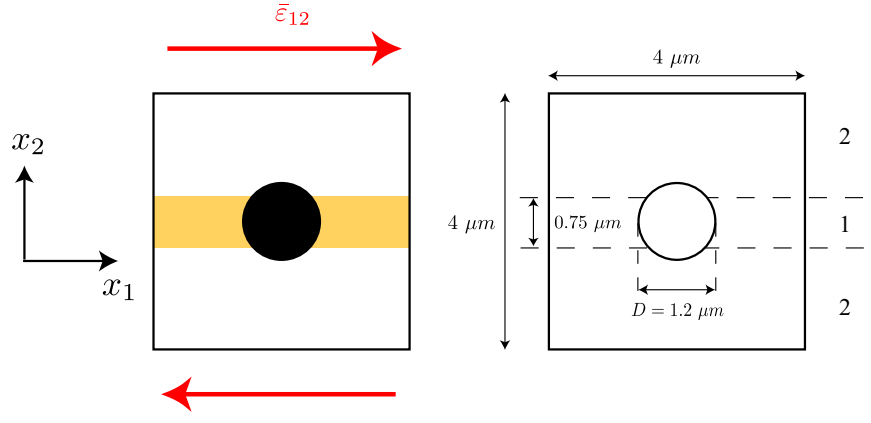

Fig. 5. Configuration considered in Case 1; the precipitate is black and initial dislocations ($\rho_- = \rho_+$) are located in the indicated band (Zone 1) only; Zone 2 is initially dislocation-free.

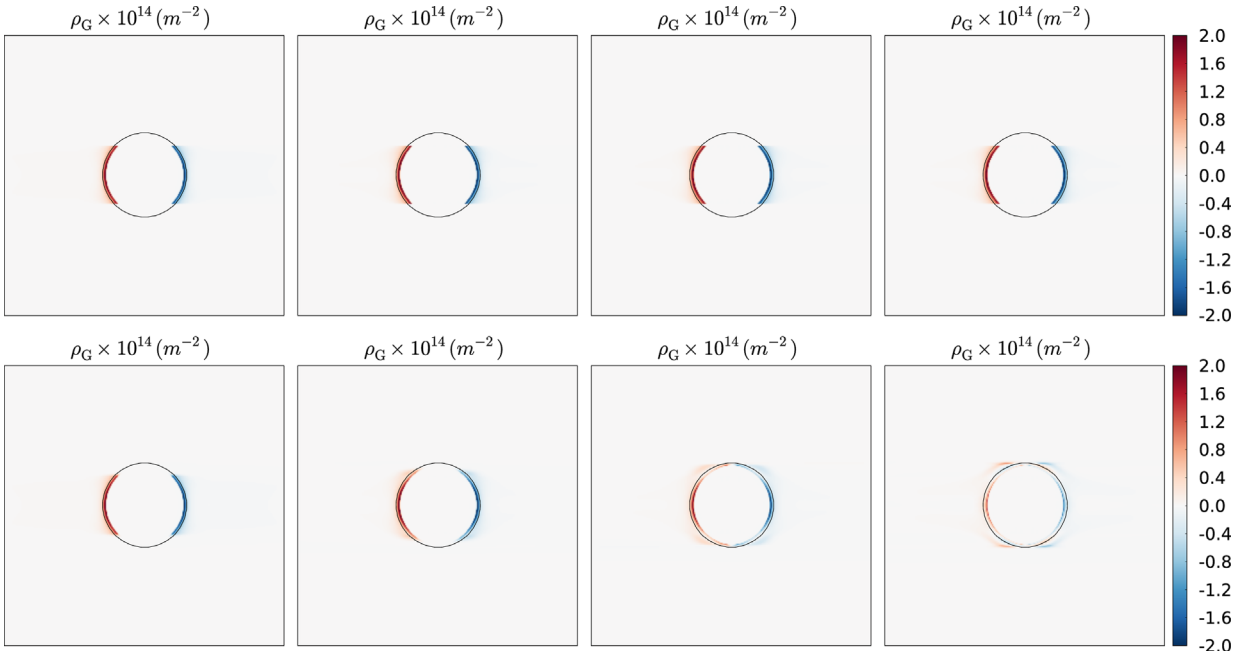

Fig. 6. Evolution of $\rho_G(\vec{r})$ at different times t=0.5, 2.0, 6.0 and 10.0 μs for the glide-only case (top) and the climb-assisted glide case (bottom). Note that there is no evolution anymore for the glide-only case, since dislocations cannot escape once the pile-ups have been formed.

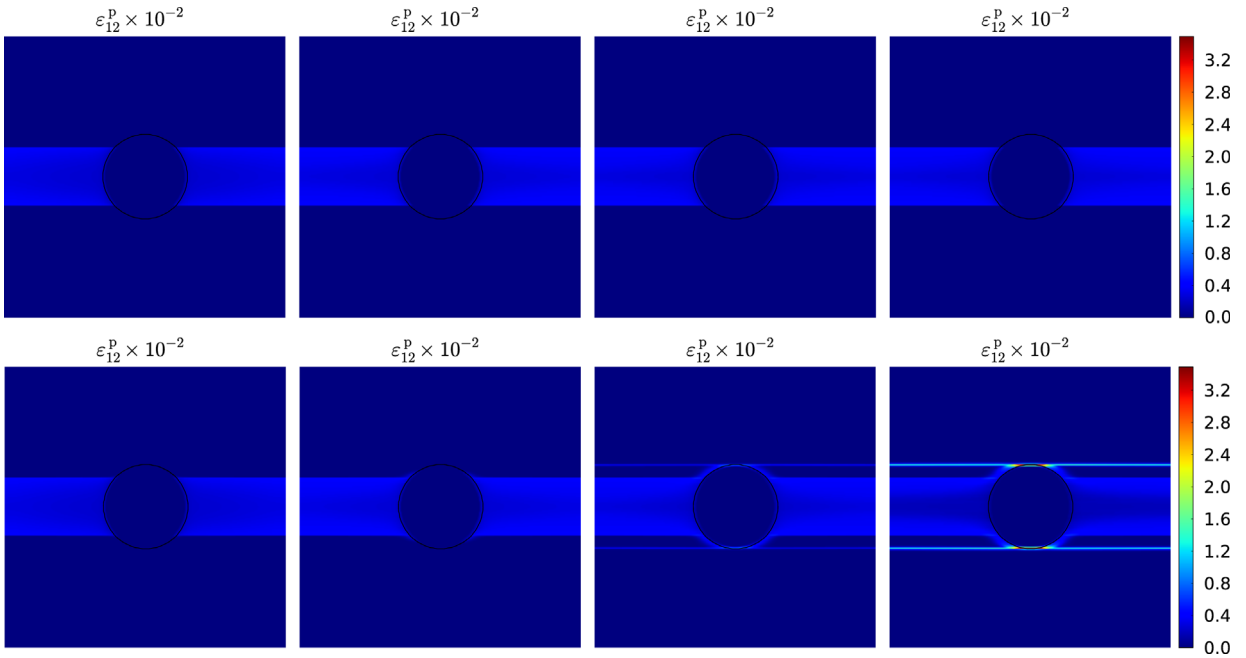

Fig. 7. Evolution of $\varepsilon^p_{12}(\vec{r})$ at different times (0.5, 2.0, 6.0 and 10.0 μs) for the glide-only case (top) and the climb-assisted glide case (bottom).

in the glide-only case. In the climb-assisted glide situation, the gradual destruction of the pile-ups entails dislocations climbing upward and downward, producing a plastic strain around the precipitate until they are able to glide again around the curved interface. Dislocations that have climbed past the precipitate enter Zone 2, where they are remobilized to glide, leading to an increase in $\varepsilon^p_{12}(\vec{r})$ with time under the applied deformation. The net result is a slightly higher plastic deformation close to the precipitate, and the formation of two parallel slip bands. Note that the plastic region near the particle in Zone 2 results from the fact that, once dislocations climb out of the pile-up, they will interact with other

dislocations and experience a different interaction stress, σ_i. As the resulting overall internal stress is reduced, dislocations therefore glide back slightly (away from the particle), which leads to a plastically deformed region of finite width around the particle in Zone 2.

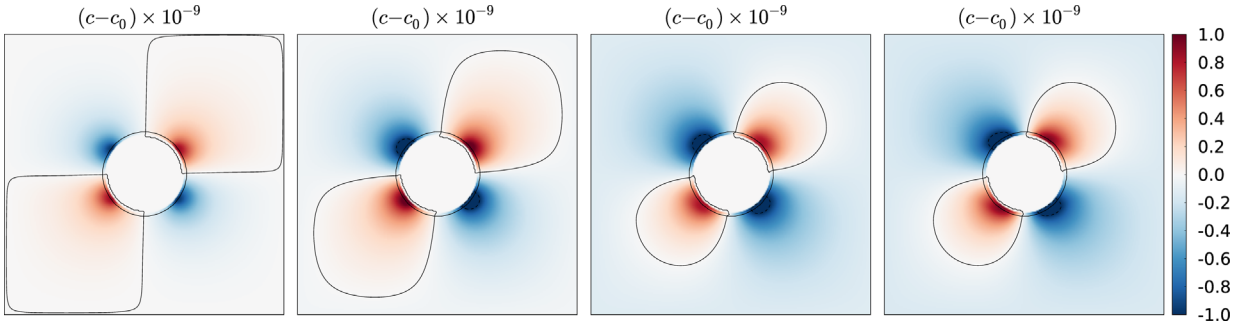

Fig. 8. Evolution of $c-c_0(\vec{r})$ at different times t=0.5, 2.0, 6.0 and 10.0 μs for the climb-assisted glide case.

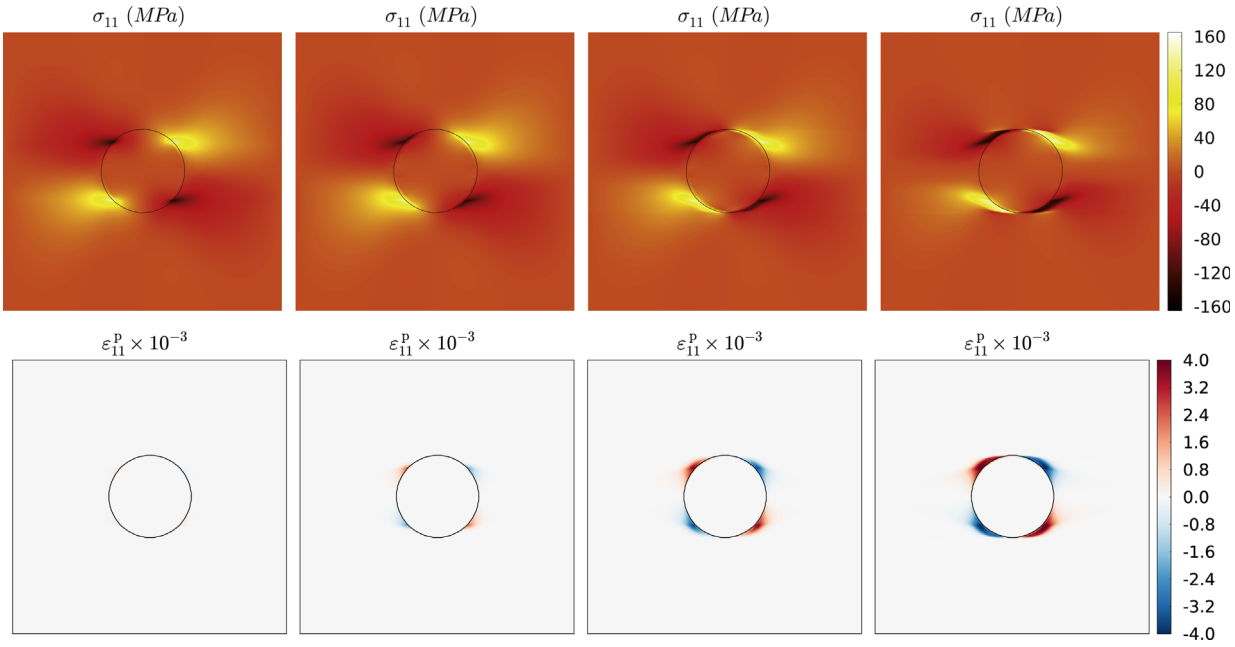

Fig. 9. Evolution of $\sigma_{11}(\vec{r})$ and $\varepsilon^{p}_{11}(\vec{r})$ at different times t=0.5, 2.0, 6.0 and 10.0 μs for the climb-assisted glide case.

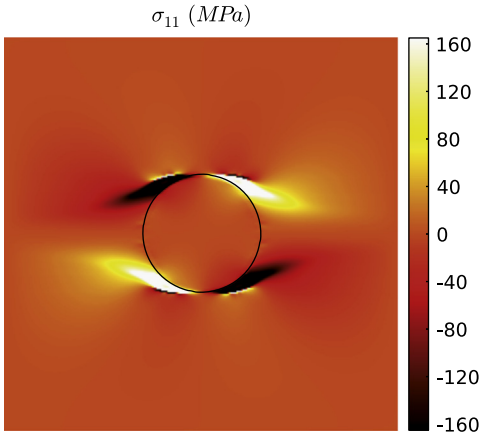

Fig. 10. Map of $\sigma_{11}(\vec{r})$ at instant $t=10.0$ μs for the climb-assisted glide case without the ε^{p}_{11} kinematical enrichment in the crystal plasticity framework.

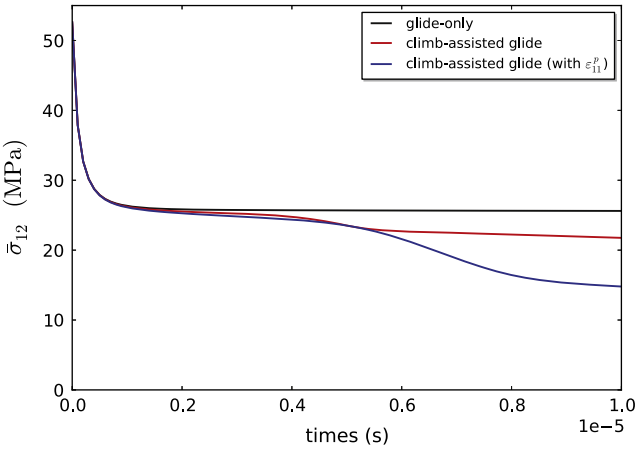

Fig. 11. Relaxation of the resulting global shear stress $\overline{\sigma}_{12}$ over time at constant applied shear: comparison of the glide-only case with the climb case.

In the climb-assisted glide case, climbing dislocations move towards slip planes in Zone 2, which is accompanied by diffusing vacancy fluxes. In Fig. 8, the difference between the local concentration of vacancies $c(\vec{r})$ and the standard state concentration c_0 is presented. In the upper left quarter of the simulation domain, there is a shortage of vacancies while there is a supersaturation in the lower left quarter. Positive dislocations situated at the left of the precipitate in Zone 1 are able to climb upward and downward around the precipitate to reach Zone 2. The resulting non-equilibrium vacancy concentration emerges from the distribution of the normal stress σ_{11}, i.e. the climb driving force. The spatially heterogeneous distribution of the normal stress σ_{11} is due to the microstructure of the two-phase material with an elastic inclusion. Positive (respectively negative) dislocation pile-ups against the impenetrable elastic walls of the precipitate generate a σ_{11} stress component that is compressive (respectively tensile) at the top and tensile (respectively compressive) at the bottom of the pile-up (Fig. 9 – top). The spreading of the pile-ups due to dislocation climb is accompanied by the evolution of σ_{11} in Fig. 9, giving rise to a local normal stress peak at the top and bottom of the precipitate.

The role of the extended climb kinematics, addressed in Section 3.2.1, is next assessed. As gliding dislocations generate a shear plastic deformation, climbing dislocations produce a normal strain ε^p_{11} due to the local variations of the vacancy concentration field. Positive dislocations climbing up introduce a tensile normal strain, as shown in Fig. 9. This kinematic contribution accompanying dislocation climb relaxes the local stresses, as may be expected. To emphasize this, the normal stress field σ_{11} for the case where the kinematic climb extension in Eq. (35) was not accounted for is shown in Fig. 10. Obviously, the stress levels reached are much higher compared to those for the climb kinematic-enriched case shown in Fig. 9 (top right). Even though the dislocation pattern obtained is not significantly affected for this particular example (not shown), the contribution of climb to the plastic strain has a strong influence on σ_{11} and therefore on the climb kinetics.

Since the imposed shear strain $\overline{\varepsilon}_{12}$ (see Fig. 5) is maintained during the entire test, the resulting global shear stress $\overline{\sigma}_{12}$ will relax over time. This is shown in Fig. 11, where the glide-only case is compared with the glide-climb case. As can be expected, the relaxation of the global shear stress $\overline{\sigma}_{12}$ is significantly enhanced by climb. The incorporation of the normal strain in the climb kinematics for the crystal plasticity model is essential, and contributes largely to the observed relaxation.

4.3. Case study 2: 2D walls

The previous example focused on the role of an elastic precipitate and the re-activation of glide once dislocations bypass the precipitate by climbing. In this second example, emphasis is given on a case where re-activation of glide is not possible and dislocation redistribution is the main outcome. This example convincingly shows how climb may have an important role in the relaxation of dislocation pile-ups. For this purpose, a 2D configuration has been chosen, which represents a periodic arrangement of elastic precipitate layers and plastic matrix channels along the x_1 direction (Fig. 12). The two-dimensional system's physical size is $\ell^2 = 2 \times 2\ \mu m^2$ (again discretized with 256^2 nodes) with precipitate layers of 0.1ℓ. The precipitate interface acts as a hard barrier for dislocations and therefore remains elastic. The elastic properties are homogeneous throughout the domain, with Young's modulus E and Poisson's ratio ν given in Table 1. The initial dislocations in the system are stored in two horizontal bands of thickness 0.16ℓ and separated by $\ell/2$ (Fig. 12). The initial total dislocation density is homogeneously distributed in these bands and equals $\rho_0 = 10^{13}\ m^{-2}$. With respect to the entire volume, this corresponds to an average total dislocation density of $\overline{\rho} = 2.9 \times 10^{12}\ m^{-2}$. As before, dislocation nucleation and annihilation are not incorporated and dislocations are relocated by transport only ($s=0$). The slip system orientation and boundary conditions are consistent with the previous example.

The spatial distribution of the GND density $\rho_G(\vec{r})$ at different times is presented in Fig. 13 for the glide-only and the climb-assisted glide case. Under the applied tensile shear strain, dislocations form pile-ups against the elastic walls with positive (resp. negative) dislocations on the right (resp. on the left). The length of the pile-ups is proportional to the shear

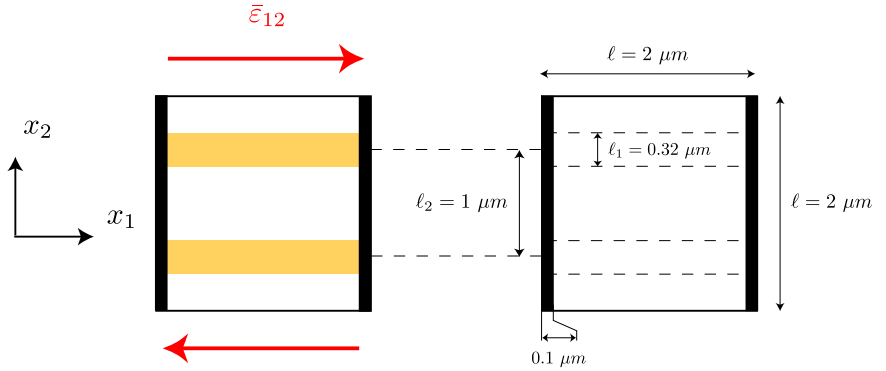

Fig. 12. Pile-up of dislocations walls.

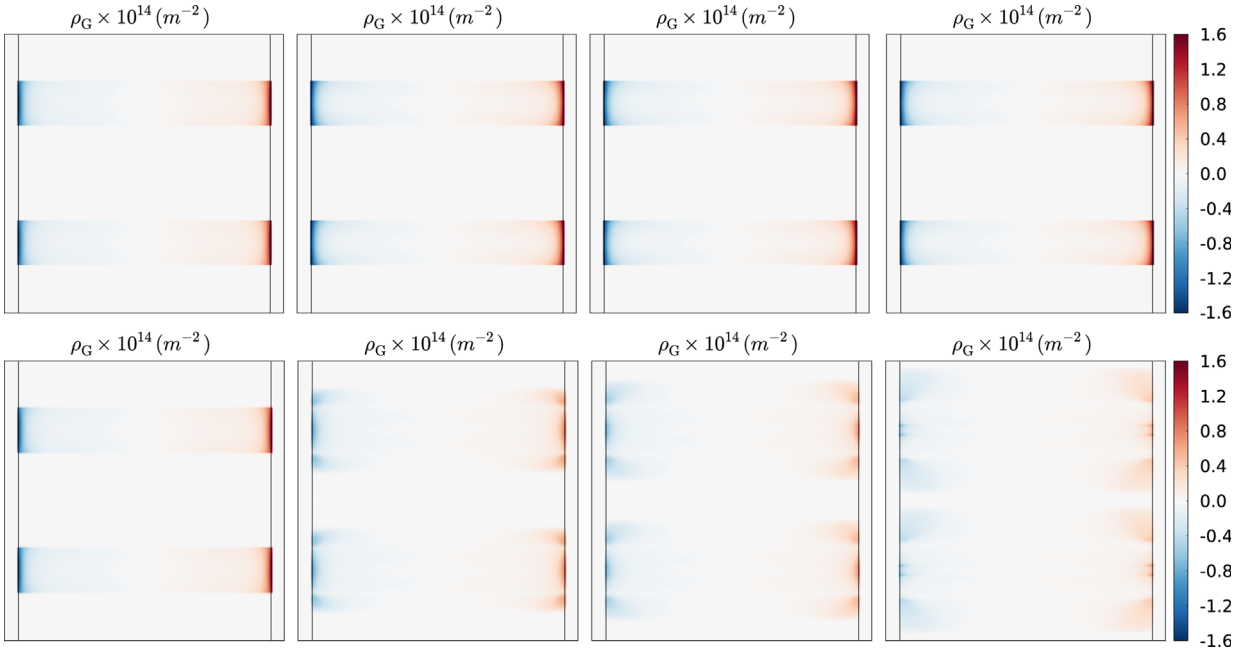

Fig. 13. Evolution of $\rho_G(\vec{r})$ at different times t=0.2, 4.8, 8.0 and 16.0 μs for the glide-only case (top) and the climb-assisted glide case (bottom).

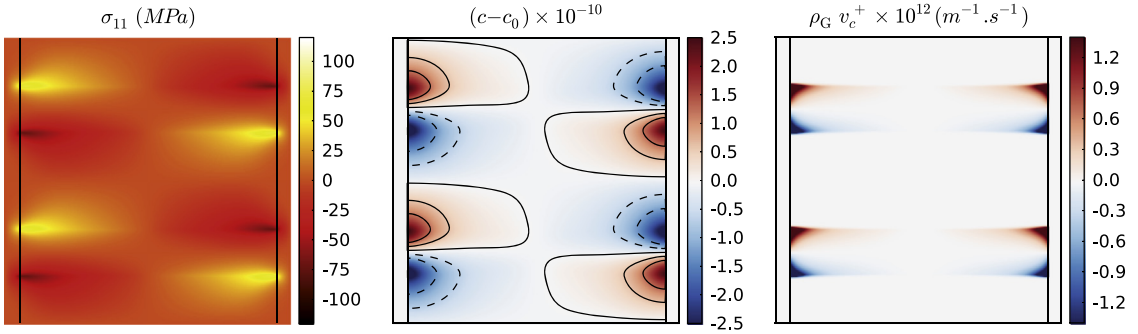

Fig. 14. Maps of σ_{11}, $c-c_0$ and the total flux $\rho_+ v_c^+ + \rho_- v_c^- = \rho_G v_c^+$ at $t = 0.3$ μs for the climb-assisted glide case.

stress and the average total dislocation density. After the second instant shown in Fig. 13 (top), the microstructure does not evolve anymore in the glide-only situation. In the climb-assisted glide, the pile-ups are spreading out vertically: dislocations at the top of the band climb upward while the ones at the bottom climb downward (Fig. 13 – bottom). The system gradually evolves to an infinite low energy wall.

The climb motion of the dislocations is again governed by the σ_{11} distribution and the accompanying vacancy diffusion. The normal stress σ_{11} at $t=0.3$ μs is represented in Fig. 14 (left). The finite pile-ups of positive (resp. negative) dislocations against the 2D impenetrable elastic walls produce a compressive (resp. tensile) normal stress at their top and inversely at their bottom. It leads to a vacancy depletion (resp. supersaturation) at the top of the pile-ups (Fig. 14 center). Therefore, the positive dislocations on the upper half of the pile-up climb upward by absorbing vacancies, triggering vacancies in the neighborhood to diffuse towards the existing gap; the positive dislocations on the lower half of the pile-up climb downward by emitting vacancies which diffuse away from the supersaturated pit. This is consistent with the dislocation fluxes in Eq. (30), presented in Fig. 14 (right).

In Fig. 15, the evolution of the plastic shear strain $\varepsilon^p_{12}(\vec{r})$ for both the glide-only (top) and the climb-assisted glide (bottom) cases is presented. The positive and negative dislocations homogeneously distributed in the two bands generate a positive plastic shear strain in these areas when gliding to reach their respective walls in the first stages of the simulation. The glide-only case saturates once the finite walls are formed. For the climb-assisted case, climb significantly affects $\varepsilon^p_{12}(\vec{r})$, whereby climb always entails subsequent glide towards the elastic wall. A negative plastic shear appears, resulting from dislocations moving backward from where they were piled-up against the precipitate walls. From the literature and Roy et al. (2008), it is known that the pile-up length (for an applied shear stress) increases if the number of dislocations in the

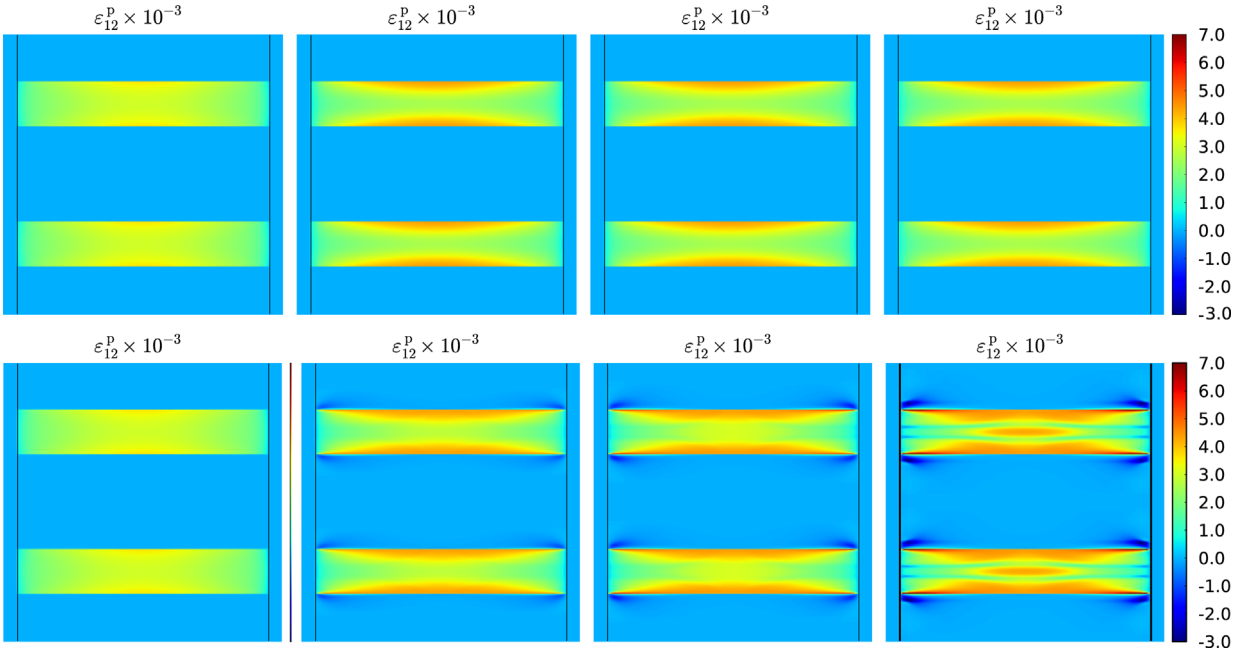

Fig. 15. Evolution of $\varepsilon^p_{12}(\vec{r})$ at different times $t=0.2$, 4.8, 8.0 and 16.0 μs for the: glide-only case (top); climb-assisted glide case (bottom).

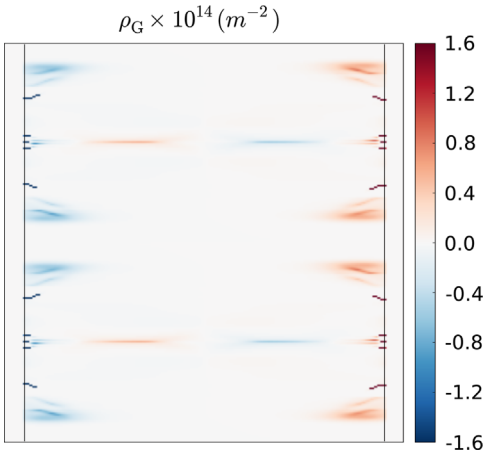

Fig. 16. Map of $\rho_G(\vec{r})$ at $t=16.0$ μs for the climb-assisted glide case obtained in a simulation where the extended climb kinematics is not accounted for ($\varepsilon^p_{11}=0$).

pile-up decreases. As the result of climb, dislocations are spreading out in the x_2 direction. Since here the total number of dislocations is conserved, less dislocations will remain on an individual glide plane, and hence they will move backward to reach their new equilibrium position.

So far, the full kinematics of the climb process (Eq. (35)) was incorporated in the presented results. In Fig. 16, the final spatial distribution of the GND density obtained without climb kinematics (i.e. ignoring the climb contribution to the plastic strain rate tensor) is shown. The repartition of the GNDs is quite different from the original (correct) one in Fig. 13 ($t = 16.0\,\mu s$) at the same instant t. Strong localization of dislocations against the wall is obtained. The omission of the ε^p_{11} contribution in the crystal plasticity framework may modify the dislocation kinetics and wrongly influence the resulting stress, strain and dislocation fields.

5. Summary and conclusion

This paper presents a fully coupled extended crystal plasticity glide-climb model, in which the deformation through dislocation glide is coupled to vacancy diffusion controlled dislocation climb. Attention is given to the governing equations and the physics of the vacancy diffusion process, the driving forces acting on a dislocation causing climb and the intrinsic coupling between both. The climb law is therefore diffusion-controlled. The problem is studied at the meso-scale, where pile-ups against particles can be resolved explicitly, i.e. a scale at which it is meaningful to preserve a direct coupling between the mean vacancy flux and the dislocation climb process. A rate-dependent strain gradient crystal plasticity formulation is adopted, which accounts for the net sign of the dislocation population. The dislocation problem is described in a fully conservative manner with transport equations. Since the analysis is carried out at the meso-scale, all dislocations are assumed to be able to participate in the climbing process. The corresponding transport equations for the dislocations are updated to incorporate climb. In order to incorporate the effect of the dislocation climb on the plastic deformation tensor, the crystallographic split of the plastic strain rate tensor is extended for the climb kinematics associated to each slip system.

The novel elements in this paper are:

- The fully coupled continuum-based vacancy-driven climb-glide theory.
- The extended diffusion problem, using a local–global approach to account for the redistribution of vacancies in the continuum sense.
- The extended dislocation transport equations, accounting for the vertical transport of dislocations across glide planes through climb.
- The extended kinematics for the crystallographic decomposition of the plastic strain rate tensor, giving rise to a crystallographic contribution of the normal strain produced by dislocation climb.

To illustrate the coupled approach and the interaction between glide and climb, two simple examples have been shown. The first concerned climbing dislocations bypassing an elastic precipitate. The second example showed how climb can relax dislocation pile-ups, by spatially redistributing the dislocations towards a low energy configuration. The theory presented is general and ready to be used in more complex 3D examples, involving multiple slip systems. The main emphasis of this paper, however, was the underlying theory, coupling and extended transport and kinematics. Further exploitation of the proposed theory and model seems well at reach.

References

Argon, A., Moffatt, W., 1981. Climb of extended edge dislocations. Acta Metallurgica 29, 293–299.
Arzt, E., Wilkinson, D., 1986. Threshold stresses for dislocation climb over hard particles: the effect of an attractive interaction. Acta Metallurgica 34, 1893–1898.
Ayas, C., Deshpande, V., Geers, M., 2012. Tensile response of passivated films with climb-assisted dislocation glide. J. Mech. Phys. Solids 60, 1626–1643.
Ayas, C., van Dommelen, J., Deshpande, V., 2014. Climb-enabled discrete dislocation plasticity. J. Mech. Phys. Solids 62, 113–136.
Bakó, B., Clouet, E., Dupuy, L., Blétry, M., 2011. Dislocation dynamics simulations with climb: kinetics of dislocation loop coarsening controlled by bulk diffusion. Philos. Mag. 91, 3173–3191.
Bakó, B., Groma, I., Gyorgyi, G., Zimányi, G., 2006. Dislocation patterning: the role of climb in meso-scale simulations. Comput. Mater. Sci. 38, 22–28.
Bayley, C., Brekelmans, W., Geers, M., 2006. A comparison of dislocation induced back stress formulations in strain gradient crystal plasticity. Int. J. Solids Struct. 43, 7268–7286.
Beddoes, J., Wallace, W., Zhao, L., 1995. Current understanding of creep behaviour of near gamma-titanium aluminides. Int. Mater. Rev. 40, 197–217.
Clouet, E., 2011. Predicting dislocation climb: classical modeling versus atomistic simulations. Phys. Rev. B 84, 092106.
Danas, K., Deshpande, V., 2013. Plane-strain discrete dislocation plasticity with climb-assisted glide motion of dislocations. Model. Simulation Mater. Sci. Eng. 21, 045008.
Davoudi, K., Nicola, L., Vlassak, J., 2012. Dislocation climb in two-dimensional discrete dislocation dynamics. J. Appl. Phys. 111, 103522.
Dobson, P., Goodhew, P., Smallman, R., 1967. Climb kinetics of dislocation loops in aluminium. Philos. Mag. 16, 9–22.
Ertürk, I., van Dommelen, J., Geers, M., 2009. Energetic dislocation interactions and thermodynamical aspects of strain gradient crystal plasticity theories. J. Mech. Phys. Solids 57, 1801–1814.
Evers, L., Brekelmans, W., Geers, M., 2004. Non-local crystal plasticity model with intrinsic SSD and GND effects. J. Mech. Phys. Solids 52, 2379–2401.
Gao, Y., Cocks, A., 2009. Thermodynamic variation approach for climb of an edge dislocation. Acta Mech. Solida Sin. 22, 426–435.
Gao, Y., Liu, Z.L., Zhao, X.C., Zhang, Z.H., Zhuang, Z., You, X.C., 2011a. Dislocation climb model based on coupling the diffusion theory of point defects with discrete dislocation dynamics. Acta Phys. Sin. 60, 096103.
Gao, Y., Zhuang, Z., Liu, Z., You, X., Zhao, X., Zhang, Z., 2011b. Investigations of pipe-diffusion-based dislocation climb by discrete dislocation dynamics. Int. J. Plast. 27, 1055–1071.

Gao, Y., Zhuang, Z., You, X., 2013. A study of dislocation climb model based on coupling the vacancy diffusion theory with 3D discrete dislocation dynamics. Int. J. Multiscale Comput. Eng. 11, 59–69.
Geslin, P.A., Appolaire, B., Finel, A., 2014. A phase field model for dislocation climb. Appl. Phys. Lett. 104, 011903.
Groma, I., Csikor, F., Zaiser, M., 2003. Spatial correlations and higher-order gradient terms in a continuum description of dislocation dynamics. Acta Mater. 51, 1271–1281.
Guo, Q., Yue, X., Yang, S., Huo, Y., 2010. Tensile properties of ultrathin copper films and their temperature dependence. Comput. Mater. Sci. 50, 319–330.
Haghighat, S.H., Eggeler, G., Raabe, D., 2013. Effect of climb on dislocation mechanisms and creep rates in gamma'-strengthened ni base superalloy single crystals: a discrete dislocation dynamics study. Acta Mater. 61, 3709–3723.
Hirschberger, C., Peerlings, R., Brekelmans, W., Geers, M., 2011. On the role of dislocation conservation in single-slip crystal plasticity. Model. Simulation Mater. Sci. Eng. 19, 24.
Hirth, J., Lothe, J., 1968. Theory of Dislocations. McGraw-Hill Book Company, New York.
Kabir, M., Lau, T., Rodney, D., Yip, S., Vliet, K.V., 2010. Predicting dislocation climb and creep from explicit atomistic details. Phys. Rev. Lett. 105, 095501.
Karanjgaokar, N., Oh, C.S., Lambros, J., Chasiotis, I., 2012. Inelastic deformation of nanocrystalline au thin films as a function of temperature and strain rate. Acta Mater. 60, 5352–5361.
Keralavarma, S., Cagin, T., Arsenlis, A., Benzerga, A., 2012. Power-law creep from discrete dislocation dynamics. Phys. Rev. Lett. 109, 265504.
Koch, C., 1998. Intermetallic matrix composites prepared by mechanical alloying—a review. Mater. Sci. Eng.: A 244, 39–48.
Larché, F., Cahn, J., 1985. The interactions of composition and stress in crystalline solids. Acta Metallurgica 33, 331–357.
Lau, T., Lin, X., Yip, S., Vliet, K.V., 2009. Atomistic examination of the unit processes and vacancy-dislocation interaction in dislocation climb. Scripta Mater. 60, 399–402.
Lebensohn, R., Holt, R., Caro, A., Alankar, A., Tome, C., 2012. Improved constitutive description of single crystal viscoplastic deformation by dislocation climb. C. R. Mécanique 340, 289–295.
Legoues, F., Copel, M., Tromp, R., 1990. Microstructure and strain relief of Ge films grown layer by layer on Si(001). Phys. Rev. B 42, 11690–11700.
Lothe, J., 1960. Theory of dislocation climb in metals. J. Appl. Phys. 31, 1077–1087.
Lothe, J., Hirth, J., 1967. Dislocation climb forces. J. Appl. Phys. 38, 845–848.
Mohamed, F., Langdon, T., 1974. The transition from dislocation climb to viscous glide in creep of solid solution alloys. Acta Metallurgica 22, 779–788.
Mompiou, F., Caillard, D., 2008. Dislocation-climb plasticity: modelling and comparison with the mechanical properties of icosahedral AlPdMn. Acta Mater. 56, 2262–2271.
Mordehai, D., Clouet, E., Fivel, M., Verdier, M., 2008. Introducing dislocation climb by bulk diffusion in discrete dislocation dynamics. Philos. Mag. 88, 899–925.
Moulinec, H., Suquet, P., 1998. A numerical method for computing the overall response of nonlinear composites with complex microstructure. Comput. Methods Appl. Mech. Eng. 157, 69–94.
Nix, W., Gascaner, R., Hirth, J., 1971. Contribution to theory of dislocation climb. Philos. Mag. 23, 1339–1349.
Ortega, M.G., de Debiaggi, S.R., Monti, A.M., 2002. Self-diffusion in fcc metals: static and dynamic simulations in aluminium and nickel. Phys. Status Solidi B 234, 506–521.
Raabe, D., 1998. On the consideration of climb in discrete dislocation dynamics. Philos. Mag. A 77, 751–759.
Rosler, J., 2003. Back-stress calculation for dislocation climb past non-interacting particles. Mater. Sci. Eng. A 339, 334–339.
Roy, A., Peerlings, R., Geers, M., Kasyanyuk, Y., 2008. Continuum modeling of dislocation interactions: why discreteness matters? Mater. Sci. Eng. A 486, 653–661.
Seidman, D., Balluffi, R., 1966a. On annealing of dislocation loops by climb. Philos. Mag. 13, 649–654.
Seidman, D., Balluffi, R., 1966b. On efficiency of dislocation climb in gold. Phys. Status Solidi 17, 531–541.
Thomson, R., Balluffi, R., 1962. Kinetic theory of dislocation climb. I: general models for edge and screw dislocations. J. Appl. Phys. 33, 803–816.
Wang, J., Hoagland, R., Misra, A., 2009. Room-temperature dislocation climb in metallic interfaces. Appl. Phys. Lett. 94, 131910.
Wang, J., Misra, A., 2011. An overview of interface-dominated deformation mechanisms in metallic multilayers. Curr. Opin. Solid State Mater. Sci. 15, 20–28.
Wang, X., Pan, E., 2011. Interaction between an edge dislocation and a circular inclusion with interface slip and diffusion. Acta Mater. 59, 797–804.
Xiang, Y., Srolovitz, D., 2006. Dislocation climb effects on particle bypass mechanisms. Philos. Mag. 86, 3937–3957.
Yefimov, S., Groma, I, van der Giessen, E., 2004. A comparison of a statistical-mechanics based plasticity model with discrete dislocation plasticity calculations. J. Mech. Phys. Solids 52, 279–300.